Non-invasive analysis of a 15th century illuminated manuscript fragment: point-based vs imaging spectroscopy

Stijn Legrand,[1] Paola Ricciardi,[2] Luca Nodari,[3] and Koen Janssens[1]

1 AXES research group, Department of Chemistry, University of Antwerp, Groenenborgerlaan 171, 2020 Antwerp, Belgium

2 The Fitzwilliam Museum, Trumpington Street, Cambridge CB2 1RB, United Kingdom

3 Consiglio Nazionale delle Ricerche, Istituto di Chimica della Materia Condensata e di Tecnologie per l'Energia (CNR-ICMATE), Corso Stati Uniti 4, 35125 Padova, Italy

Abstract

Illuminated manuscript fragments are some of the best preserved objects of Western cultural heritage. Therefore, scholars are limited to non-invasive - often point-based - methods, to answer questions on material usage, technique, origin and previous treatments. These powerful methods yield specific information; however, the information is limited to the number of points analyzed. Imaging spectroscopies such as MA-XRF and MA-rFTIR combine specificity with the power of imaging, resulting in distribution images that are interpretable by non-spectroscopists and the public at large. In this paper the possible added value of using imaging spectroscopy is discussed. Do these methods yield the same results as an extensive point-based spectroscopic campaign and can they bring novel information? As a case study, a 15th century illuminated manuscript fragment is employed in order to explore the differences between these approaches and present an inventory of their advantages and limitations.

Keywords

Illuminated manuscript, MA-XRF, MA-rFTIR, chemical imaging, hyperspectral imaging, non-invasive analysis

1. Introduction

Of all objects of Western cultural heritage, Medieval and Renaissance manuscript illuminations have most frequently retained their original color appearance in an optimal manner. Often well protected within volumes, inside their heavy bindings, they were less exposed to environmental variations, pollutants, vandalism and other causes of damage and degradation. As a result, they can provide scholars with detailed insights into Medieval and Renaissance artists' materials and techniques, showing geographic variation as well as their evolution over time.

Due to their smaller size and generally better state of preservation than easel paintings, sampling of illuminated manuscripts is rarely allowed. Thus their scientific analysis has to be limited to non-invasive techniques. Point-based techniques such as X-ray fluorescence (XRF) spectroscopy, Raman spectroscopy and ultraviolet visible and near-infrared (UV-vis-NIR) fibre optics reflectance spectroscopy (FORS) are all routinely employed for this purpose [1,2,3,4,5]. Microspectrofluorimetry and X-ray diffraction have also been used successfully in several cases [6,7,8,9]. One of the oldest and most widely used imaging methods for the examination of works of art is X-ray radiography (XRR). Contrary to the case of easel paintings, XRR is used much less frequently to investigate illuminated manuscripts due to the thinner build-up of the paint layers and the lower occurrence of significant pentimenti. The use of NIR reflectance (IRR) and UV (fluorescence) imaging systems has long allowed scholars to visualize underdrawings and to identify past conservation treatments. More recently, hyperspectral imaging systems have become an appreciated set of tools in the field of cultural heritage science. Originating from the field of remote sensing [10], such systems record reflected or emitted UV, visible and NIR radiation in a large number of narrow contiguous spectral bands, resulting not only in (hundreds of) images, but also in a full spectral response curve to become available at each imaged pixel [11,12,13,14,15]. The most recent generation of hyperspectral imaging systems not only employs camera systems, but often incorporates spectroscopic techniques such as FORS, XRF, XRD, and FTIR also used in scanning mode [16,17,18]. Methods of this type that are employed in this paper

are macroscopic XRF (MA-XRF) [19,20] and macroscopic reflection mode FTIR (MA-rFTIR) scanning [21].

The main purpose of this paper is to describe which additional benefits can be obtained by collecting a combination of spectroscopic data across the entire surface of the work of art, rather than limiting the (multimode) spectroscopic analysis to a discreet number of locations that are considered *a priori* to be representative of the entire artefact. To do so, we will consider a 15th century illuminated manuscript fragment (Fig. 1), which had initially been characterized by means of various point-based spectroscopic methods, allowing to make a (hopefully) complete list of the paintings materials employed for its creation in a non-invasive manner. The fragment was recently part of a major exhibition at the Fitzwilliam Museum [22], in preparation for which scanning MA-XRF and MA-rFTIR analyses were performed in Cambridge during two successive measurement campaigns in 2014 and 2016.

By selecting a fragment from a 15th century illuminated manuscript as a case study, rather than a more complex artwork such as an oil painting, we opt to investigate an object with a simpler layer stratigraphy and in which less complex pigments mixtures are presumably employed. These two factors should allow to focus on the problem of pigment identification via a multi-modal spectroscopic approach, while avoiding limitations imposed by the presence of covering varnishes, oily binding media and overpaint layers that strongly absorb and scatter radiation.

We will first discuss the information which can be gleaned from the elemental maps generated by means of MA-XRF imaging of the fragment. In addition to the elemental maps themselves, we will show that employing inter-element correlation among MA-XRF distributions can be very useful to distinguish between various types of artists' pigments having similar but (sometimes subtly) different elemental profiles. Since this approach does not always suffice to extract all relevant information on the nature of the materials present, we will then discuss the combined use of MA-XRF and (reflection mode) MA-FTIR to obtain maps with higher chemical specificity. We will conclude by making a critical assessment of the advantages and limitations of the combined use of

MA-XRF and MA-FTIR when compared to point-based multimodal spectroscopic materials identification.

2. Materials and Methods

2.1. The manuscript fragment: St Clement in a historiated initial D

The manuscript fragment studied (Fitzwilliam Museum, MS 5-1979, Fig. 1) shows St Clement in a historiated initial D. It is one of four initials in the Fitzwilliam Museum's collection which were originally part of a set of choir books illuminated between 1370 and 1506 by successive generations of artists in the scriptorium of the Camaldolese monastery of Santa Maria degli Angeli in Florence [22]. These volumes were mutilated during the Napoleonic campaigns (1797-1809), with many of their images cut out to be sold as individual 'paintings' and therefore subsequently scattered all over the world. The volumes remain at the Biblioteca Laurenziana in Florence, labelled as *Corali* 1-19. The image with St Clement was excised from *Corale* 2, the earliest work of the head of the scriptorium Don Silvestro dei Gherarducci, dated to 1370-1371. The initial would have opened the Introit to the Mass for St Clement's feast on November 23rd beginning *Dicit dominus sermones mei*, originally on folio 159 of the book [23]. When excised from its parent book, the initial, measuring approximately 150 x 145 mm, was trimmed very closely to its edges (the entire fragment only measures 170 x 165 mm) and then glued to a cardboard support, which currently obscures the reverse side.

2.2. MA-XRF instrumentation

MA-XRF is based on the sequential recording of a very large number of XRF spectra while a two-dimensional motorized stage moves the artwork relative to the measuring head, or vice versa. The latter consists of (a) an X-ray tube equipped with either a collimator or a polycapillary lens to define the primary X-ray beam and (b) one or more energy-dispersive detectors to record the XRF signals emitted by the irradiated spot on the work of art. Due to the relative low energy of the secondary X-rays, measurements must be performed in reflection mode: the X-ray source and the detector capturing the secondary X-rays are positioned on the same side of the object.

Using such a setup, distribution information can be obtained for chemical elements heavier than K. Lighter elements such as S, P, Na, Mg, and Si emit low energy XRF signals (< 3 keV), which are significantly absorbed by the object itself and in the air path between object surface and detector. Another limitation of the method is related to the use of energy dispersive (ED) detectors, which have a broader energy resolution than the intrinsic bandwidth of the secondary X-rays. This causes overlaps between element-specific XRF signals with approximately the same energy levels. Careful evaluation of the spectra by fitting them to analytical models allows to resolve most of these overlaps, but may lead to artefacts in the resulting images if the overlap is not correctly dealt with.

The MA-XRF scan recorded in this work was obtained using version F of a dedicated instrument, described in detail elsewhere (Fig. 2a) [20]. This instrument consists of a 50 watt molybdenum anode X-ray tube (XOS, USA), equipped with a polycapillary lens with a focal spot size of 50 µm at a distance of 3 mm. During scanning, the manuscript fragment was placed parallel to the scanning plane at a distance of approximately 6 mm from the front of the lens, resulting in a larger spot size than defined by the polycapillary. The tube ran at 50 kV and 1 mA, with a dwell time of 365 ms and a step size of 333 µm. One Vortex EX-90 detector (Hitachi, USA) was used, at an angle of 50 degrees relative to the primary beam.

With MA-XRF, the measuring head consists of an X-ray tube and an energy-dispersive X-ray detector; every 0.333 mm, an XRF spectrum is recorded during a period of 0.365 s, resulting in an overall scanning time of 22 hours.

The MA-XRF dataset was processed by means of a combination of three data processing packages: Datamuncher [24], PYMCA [25] and bAXIL [26,27]. The results of this data treatment are three dimensional (x,y,E) data cubes, where x and y are the spatial or pixel coordinates of the scanned area. The third dimension (E) represents the net XRF intensities of the different elemental contributions (Z>15) to the recorded XRF spectra. Figure 3 shows a series of elemental maps recorded from the manuscript fragment.

For more quantitative analysis and in order to distinguish between multiple combinations of the same two elements, correlation biplots can be used (see e.g. Figs.

6 and 8). In these graphs, each pixel is plotted against its fitted intensity for two elemental lines. If there are multiple pixels with a similar composition, these will appear correlated and can be seen as clusters. By selecting these clusters, it is possible to mark the corresponding pixels in an elemental distribution image.

2.3. MA-rFTIR instrumentation

MA-rFTIR also works in a point-by-point scanning mode; it operates in the mid infrared range. The measurement head, a compact Alpha FTIR spectrometer (Bruker, Germany) [21] emits a polychromatic beam of infrared radiation of 1-2 mm diameter via the Michelson interferometer. This beam is focussed on the surface under examination by a spherical gold mirror. A second mirror of this kind captures the radiation reflected by the surface and leads it toward the DTGS detector of the FTIR spectrometer. A $2o^0/20^o$ irradiation/collection geometry is employed. Due to the low energy of infrared radiation, for most of the artists' materials present in illuminated manuscripts, it has much lower penetration capabilities than X-ray radiation. In order to use this technique in a non-invasive manner, it has to be applied in reflectance mode (contrary to classic IR-spectrometers which usually operate in transmission mode). The resulting reflected infrared spectra are more complex than regular absorption FTIR spectra, as absorption bands can appear inverted or show a derivative shape [28].

Figure 2b shows a photograph taken during the MA-FTIR scanning of the manuscript fragment. Spectral acquisition was done using the Bruker OPUS 6.0 software package in the range 7500 - 375 cm^{-1} (~ 1.3 – 26.7 µm). A spectral background was recorded during 30 minutes prior to scanning the manuscript fragment by placing a gold coated mirror in front of the instrument. A coaxial camera allowed to monitor the scanning process and helped with the alignment of the instrument with the artefact. The fragment was placed in the instrument's focal point at a distance of 1.5 cm from the external reflection module. During a scan, an FTIR spectrum was recorded each millimetre over a period of three seconds, resulting in a total scanning time of 56 hours.

All subsequent MA-rFTIR data treatment was performed in the scientific programming package IDL 8.3. Individual FTIR spectra were converted into a three dimensional data cube, with x and y being the spatial coordinates and z the measured reflectance

intensity. The reflectance intensities (R) are converted to pseudo absorbance (A'=log(1/R)). The chemical distribution images display the baseline-subtracted, integrated intensity of the infrared band of interest. This subtracted baseline runs through the first and the last point of the integrated interval. In order to obtain qualitative spectra for identification, nine spectra from similar data points are combined when extracting spectra from the dataset in order to reduce the noise that is inherently present when measuring only briefly in each point.

3. Results and discussion

3.1. Preliminary results

Table I shows an overview of pigments present in the differently colored areas of the fragment, identified using a combination of non-invasive site-specific techniques including FORS, XRF, FT-IR and Raman spectroscopy accompanied by near-infrared imaging and observation under magnification. This work was carried out prior to the macro-scanning experiments [29]. The palette is fairly standard for 14th century Florentine illumination and includes carbon black, lead white (used both on its own and mixed with other pigments to modify their hue), vermilion, red lead, ultramarine, azurite and organic pinks. Small amounts of ultramarine were also added to the white areas in order to obtain a cooler hue. A dark red earth pigment was used to outline the glittering bronze-coloured decorations painted in mosaic gold (SnS_2). A yellow lead oxide (PbO, massicot) was likely mixed with azurite to provide green hues whereas the yellow oval surrounding St Clement was painted with lead-tin yellow. Gold leaf was laid over a gypsum-based ground and a red bole and then burnished to a high shine. The flesh tones were painted by mixing and layering different amounts of lead white and vermillion on a green earth base, using a technique that closely resembles contemporary easel painting. Egg yolk appears to have been used as a binding medium for the red lead paint, and possibly for vermilion as well [30,31].

colour	pigments
black	**carbon-based black**
white	**lead white (ultramarine mixed in)**
red	**vermillion** **red lead (orange hue)** **Fe-oxide pigment**
pink	**gypsum, organic dye**
yellow	**lead-tin yellow (type II?)** **lead oxide or lead white and organic dye**
blue	**ultramarine, azurite** **ultramarine**
green	**azurite mixed with lead oxide or lead white and organic dye**
flesh tones	**green earth, lead white, vermillion**
metals	**gold** **mosaic gold**
bole	**gypsum, Fe-oxide pigment**
ink	**(brown) Fe-gall ink** **(red) vermillion**

Table I. Palette identified on MS 5-1979 prior to MA-XRF and MA-rFTIR scanning.

The pink leaves and the yellow initial, as well as the white highlights over the orange leaves and ornaments, have darkened significantly. This is most likely linked to the presence of lead white. In the pink and yellow areas the discoloration appears to have started not on the surface but rather in the lower portion of the paint layers. If this is indeed the case, the degradation process may have been catalyzed by the materials used to glue the fragment to its modern cardboard support. Microscope images acquired in raking light provide evidence of the previous existence on the front side of the image of a brown cardboard mat, stamped with flowers and other decorative elements. The impressions left by these flowers are still visible, especially along the lower edge of the fragment.

The following paragraphs discuss in detail the artists' materials and techniques used for the decoration of the manuscript fragment and focus specifically on how these can be identified through a combination of different MA-XRF and MA-rFTIR images.

3.2. Gilded areas

With respect to the gilded parts of the fragment, several questions can be answered by means of chemical imaging: what type of gilding method was used? Is real gold actually employed in all areas which appear gilded? What is their overall state of conservation?

As shown in Table I, metallic gold (Au) is present, predominantly in the background of the fragment but also to depict the gilded edge of the saint's robe. A form of imitation gold is also present, in the roundels above and below the saint and in the shiny bronze-looking leaf in the top left corner. This is tin sulphide (SnS_2), usually called 'mosaic gold'.

In the 15th century, illuminated manuscripts were gilded either by painting with 'liquid' gold (so-called 'shell gold') or by applying thin gold sheets ('gold leaf'). Shell gold was prepared by grinding small gold flakes in a shell and by mixing the resulting powder with a binding medium, after which it could be used as regular paint. In order to make thinly hammered gold foils adhere to a manuscript page, a colored preparatory layer was usually painted first onto the parchment substrate. This facilitates adhesion of the gold foil and also allowed to modify its color, shape and surface texture and permitted burnishing of the surface. Figure 4a represents a schematic cross section of gold leaves (yellow) applied using a bole (red) on parchment (brown). From left to right, along the top, one can see first the most common situation with a single leaf present; followed by a damaged area where the bole is exposed; then details painted in blue and orange on top of the gold leaf (as is the case e.g. along the edge of the Saint's mantle); and finally a double layer of gold, indicating areas where two leaves overlap.

The Au-L maps in Figures 3 and 5d illustrate how MA-XRF can be used to specifically identify the gilding technique used. In those areas where two gold foils were made to overlap, the Au-L intensity is approximately twice as high as that observed in other gilded areas (yellow areas in Figure 6a). In the Au-L map, the location of the multi-colored decorations painted over the gilded edge of the robe are visible as darker spots, since the painted-on details partially absorb the Au-L XRF signals emerging from the gold foil (see Figures 3 and 5d). The Fe and Ca maps in Figure 4 allow to see that wherever gold leaf was employed, faint Ca-K and Fe-K signals are also present,

emerging from the bole layer used as a ground for the gold foil. In both of the maps, where a double thickness of gold leaf is present, the signal from calcium and iron is lower, confirming that these two elements are situated in a paint layer below the gold. Small areas of gold leaf loss (Figure 5a) can be identified as bright 'spots', especially visible in the Ca-K map, and marked in red in the false-color image shown in Figure 5b. The same areas in the gilded background that appear as hotspots in the Ca-K map, show an increase in intensity for the sulphate stretching band visualized in Figure 4e, supporting the presence of gypsum in the bole layer as can be seen in the proposed cross-section in Figure 4a. This gypsum can only be detected when the gold layer is damaged, as the thin gold foil otherwise reflects the IR radiation before it can reach the underlying gypsum.

When considering the Au-L, Ca-K and Fe-K distributions more in detail, for example in the upper left portion of the gilded background, above the initial D, it becomes also clear that these elemental images can be used to map and quantitatively estimate the fraction of the leaf-gilded area that has lost its gilding. These areas can be identified by employing the Au-L vs Ca-K XRF intensity scatter plot of Figure 6b. In this scatter plot, two main features can be seen: a narrow vertical cluster (circled in blue, on the left) consisting of pixels showing no gold and an large group of pixels featuring an anti-correlation between gold and calcium. This anti-correlation means that with increasing Au-L intensity, the detected Ca-K intensity decreases. The bulk of the pixels in this anti-correlation groups - circled in green and corresponding to areas covered with a single gold leaf - appear over a net Au-L intensity range of 600 to 1700 counts. Another group (in red), which contains a relatively small number of points, appears to be an extension of the green group towards lower Au-L intensities; this group corresponds to areas where the gold leaf has detached. Above 1700 net Au-L counts, a different anti-correlation between Au-L and Ca-K is observed, suggesting that the stratigraphy is different than in the above-described areas; the resulting group of pixels, circled in yellow, represent areas where two gold leaves overlap. These four color-coded pixel groups are shown in the form of a false color image in Figure 6a (where the white rectangle indicates the detail shown in Figs. 5a and 5b). The "red coded" pixels in the background area amount to ca 6% of the total single leaf-covered area (green in Fig.

6a). As mentioned above, the “red coded” pixels are characterized by a higher Ca signal, since in these locations the gold leaf that absorbs the Ca-K XRF signal is no longer intact. Other Ca-rich pixels in areas that do not contain gold are “blue coded” and relate to the blue initial “D” surrounding the saint rather than to the gilding.

Areas painted with mosaic gold, characterized by the presence of Sn, can easily be identified from the (higher intensity portions of) the Sn-L map in Figure 3 and the blue color-coded pixels in Figure 8c. The small gilded portion of the robe’s edge next to the saint’s proper right hand also appears to be painted in mosaic gold instead of real gold, and shows no bole preparation either (virtually no Ca or Fe are present). Gold leaf was usually applied first, before the rest of the decoration was painted. The artist must have realized belatedly that this area needed to appear gilded, and used mosaic gold to simulate the appearance of the precious metal which he had forgotten to lay down. All mosaic gold elements of the illumination are outlined with a Fe-rich, dark reddish paint, which can be identified as red earth by the presence of hematite and clay minerals in the FT-IR maps. The fact that sulfides [32,33] and presumably mosaic gold as well can act as a local source of H_2S, a gas which can react with lead white to form galena (black lead sulfide, PbS) [34,35] might help explain the black degradation product that has formed on top of the white highlights over the orange decorations (Figure 5e).

From these considerations it is possible to conclude that in addition to the nature of the materials employed for gilding, the distribution of real and imitation gold conveys information on the specific techniques of application of these materials. As shown by Turner et al. [36] also the size and shape of the individual gold leaf squares employed can be estimated in this manner.

3.3. Information from the reverse side

Since MS 5-1979 was originally part of a choir book, it is not surprising that a musical score is present on the reverse side of the fragment. This can be observed in the Fe-K, Zn-K and Hg-L maps (see Figure 7), even though the fragment has been glued over thick cardboard. These maps correspond to fairly energetic XRF radiation (6.4 keV for Fe-K_a, 8.6 keV for Zn-K_a and 9.99 keV for Hg-L_a) so that when irradiating the parchment fragment, painted on both sides, the XRF radiation from both the recto and the verso

can reach the XRF scanner detector without being completely absorbed along the way. The Zn and Hg maps can be read as a superimposition of contributions from both painted surfaces, on the recto and on the verso. Contributions from the recto include the green acanthus leaf in the lower right corner, visible in the Zn map, which are linked to zinc impurities in the azurite blue pigment used in the green mixture. Vermilion red dots, which decorate the saint's paraments, are visible in the Hg map. Also visible are traces of mercury in the areas painted with mosaic gold; these are remnants of the starting material used for the preparation of this synthetic pigment. Once these contributions are taken into account, one can identify what is present on the reverse side: in the Hg-L image, vermilion red musical lines are clearly visible, whereas the Zn-K image clearly shows lettering as well as square and diamond-shape musical notes. Zinc is a common impurity in ferro-gallic inks, used for the text and musical notation in the majority of medieval and Renaissance illuminated manuscripts in Europe. One would expect to be able to identify the same lettering and musical notes in the Fe-map where, however, these contributions from the verso are not at all well visible. This is a common problem, also observed in other manuscript fragments (see for example the other three objects shown at http://www.fitzmuseum.cam.ac.uk/illuminated/manuscript/discover/initials-from-choir-books). It is partly due to the contribution of Fe signals originating from the green earth underpaint of the saint's face and beard of the saint, the above-mentioned hematite used to outline the mosaic gold areas and to paint the mitre's lappets, and the red clay used as a ground layer for the gold leaf. The intense Fe-signals emerging from the recto side combined with the object's stratigraphy, with rich paint layers as well as gold leaf, result in a recorded intensity for Fe which is lower than would be expected for iron gall ink. It is however still partially possible to visualize the lettering on the verso, by adjusting the grey scale of the Fe-K map to maximize the lower intensity levels, shown in Fig. 4c.

The Zn map, which contains the most information about the text on the reverse of the fragment, can be horizontally mirrored and contrast-adjusted to improve its readability (Figure 7b). It is thus possible to read the Latin text: "s vir sāc" on the first line, followed by "s Urbis tu" on the second one. Considering the presence of missing text on both the left and the right side, the entire sentence can be read as "[Beatu]s vir sa(n)c[tus

Martinu]s urbis tu[tonis Episcopus]", or "Beatus Saint Martin Bishop of the city of Tours". This is a significant discovery, as it allows to confirm the position of the St Clement fragment within its parent book, and to establish that the image was originally on the verso of a page [37].

These observations clearly show that in addition to providing information on the visible side of an illuminated fragment, a MA-XRF investigation is occasionally also able to provide relevant data of the reverse, often inaccessible side, which may reveal significant information about the origin and original context of the object. At the same time, it should be pointed out that this advantage of the method, sometimes is also a limitation: in the case of illuminations in a bound volume being examined, care must be taken to isolate the illustration under examination from those on the adjacent pages in order to eliminate unwanted contributions from neighboring folios. This can be done by placing e.g. a lead sheet below the page being scanned or by suitable positioning of this page relative to the rest of the book.

3.4. (Un)specific mapping of lead-based pigments of different colours

Figure 8b shows the MA-XRF distribution map of Pb, obtained by recording the Pb-L XRF radiation. A comparison with the visible image of the fragment (Fig. 1) shows that lead is present, in variable amounts, in all non-gilded areas and thus corresponds to white, yellow, red, pink, green, blue and flesh-colored areas. Clearly the filigree details painted on top of the mosaic gold areas and the blue exterior of the initial D appear to be painted with lead white. However, the nature of the other lead compounds present is not immediately obvious. The Pb-L - Sn-L correlation biplot of Fig. 8a (with the pixels mapped in Fig. 8c) allows to distinguish at least three subgroups: the blue pixel cluster corresponding to a high Sn-L signal but very low Pb-L signal, corresponding to the mosaic gold areas; the yellow cluster, situated just above the main (red color-coded) cluster, corresponding to areas where the Pb dominates over the Sn-L signal, but the latter is not zero. These pixels correspond to the inner part of the initial D, which was painted with lead tin yellow type I ($PbSnO_4$) or type II ($Pb(Sn,Si)O_3$). Finally, the largest cluster of pixels shows a high Pb-L signal, without detectable Sn-L response. This

corresponds to the mitre, the stole, the alb and the book. It also includes the orange leaves and decorations surrounding the initial.

While it would be reasonable to suppose the presence of minium in these orange-red lead-based areas, it is not possible to derive the distribution of this pigment from the MA-XRF maps of Pb alone. In order to distinguish lead white ($PbCO_3$ and/or $2PbCO_3.Pb(OH)_2$) from minium (Pb_3O_4) the FTIR distributions of Figures 8d and 8e must also be considered. Fig. 8d shows the intensity of the stretching vibration band (680-720 cm^{-1}) of the carbonate group attached to a Pb^{2+} ion [38,28], while Fig. 8e maps the intensity of the Pb-O stretching band (530-585 cm^{-1}) [39], characteristic for minium, confirming that this pigment was used to paint the book cover and some of the acanthus leaves and other marginal decorations. The images of Figure 8 allow to clearly map the distribution of the various lead-bearing species, in a manner which is consistent with the visible colours of the illumination. Although the spatial resolution of the FTIR maps is not high enough to reveal all the fine details of the painting, the map in Fig. 8d does correspond very well to the lighter areas of the fragment, where lead white is either present by itself (e.g. in the white draperies and paraments, the flesh tones, and in the filigree decoration over the blue initial and the orange and mosaic gold areas) or mixed with red lakes in the pink acanthus leaves in the upper right and lower left corners).

3.5. Mapping of blue pigments: azurite and ultramarine

In the blue parts of the initial, several colour tones can be distinguished, ranging from the pale blue of the background to the darkest blue outlines (Figure 9a). Figure 9b shows a virtual cross-section of the blue initial, based on the MA-XRF results. A pale blue base layer was applied on the parchment. White details were applied on top of this layer, while the darker hues were obtained by superimposing multiple blue brush strokes over the base layer.

As shown in Figure 9c, the blue initial shows a quasi-uniform Cu-K XRF intensity, with the exception of the areas where the signal is strongly absorbed by the superimposed lead white filigree patterns. This would suggest that an azurite base layer was painted for the initial as a whole. It is worth noting that in the blue portions of the saint's clothing,

no Cu and therefore no azurite is present, with the exception of the small green decorations (see Cu-K map in Figs. 9c and 11c).

The Ca-K image (Fig. 9d), on the other hand, shows a distribution similar to the visible image, with lighter areas emitting a higher Ca signal, suggesting the use of chalk or gypsum. This could misinterpreted as if this Ca was used to create a lighter blue. However, careful comparison of the Ca-K, Cu-K and Pb-L distributions (Figs. 11a,c,e) shows similar brush marks for all three elements, an indication that these are all present in the same (base) layer. The relative low energetic Ca-K XRF radiation is absorbed to a higher degree than the more energetic Cu-K and Pb-L radiation by the K-rich pigment in the dark blue parts.

The overall K-K MA-XRF map in Fig. 10a shows that both the blue mantle of the saint and the darker tones in the blue areas of the initial (Figure 9e) were painted with a K-containing pigment, which is likely to be natural ultramarine (see Table I). Since the K-K intensity does not drop down to zero in the pale blue circular holes, probably some ultramarine was already mixed with the azurite base layer. (Since low energetic K-K radiation is significantly absorbed by the ultramarine paint layers themselves, the K-K image does not reflect the thickness variations among the ultramarine brushstrokes present.) However, since the presence of the element potassium is only consistent with, but not conclusive proof for, the presence of ultramarine, the MA-FTIR data were examined to seek confirmation. This could be found in three spectral regions within the FTIR datacube. The MA-XRF K-K distribution (Fig. 10a) turns out to be very similar to the intensity map of the FTIR band at 2317-2362 cm^{-1} (Fig. 10b) which can be regarded as a specific signal for Afghan ultramarine. As described by Miliani et al. [40], a distinctive sharp peak at 2341 cm^{-1} can be observed (Fig. 12a) and attributed to the presence of CO_2 in the aluminosilicate cages of the mineral lazurite. Another interpretation for the origin of this peak is that it is caused by vibration of HS_3^- species inside the aluminosilicate cages [41]. While the FTIR map is more blurred than the K-K XRF map due to the larger beam employed during FTIR scanning, taken together, the two distributions clearly indicate that natural ultramarine was used in all blue areas of the illumination, and consistently with the layer structure schematically shown in Fig. 9b.

Additional FTIR maps support the identification of ultramarine in these areas: the presence of silicate-rich material is confirmed by the intensity distributions of the bands at 460-530 cm^{-1} (Si-O bending vibration, Fig. 10d) and at 960-1050 cm^{-1} (Si-O stretching vibration, Fig. 10e).

3.6. Florentine green: an azurite mixture

Figure 11 shows the XRF- and FTIR-derived distributions of three metal-carbonate species, i.e. chalk ($CaCO_3$), azurite ($2CuCO_3.Cu(OH)_2$) and lead white – here assumed to be predominantly present in its hydrocerussite form, $2PbCO_3.Pb(OH)_2$, based on the clear –OH signal observed at 3540 cm^{-1} (data not shown). The direct comparison between the XRF and FTIR maps shows that all Cu (Fig. 11c) appears to be present as azurite (Fig. 11d) whereas, as already discussed above, Ca and Pb are also present as chemical species other than carbonates. The main difference between the Ca map of Fig. 11a and the chalk map of Fig. 11b appears to reside in the gilded background and in the pink-colored acanthus leaves where $CaSO_4.2H_2O$ is present, respectively in the bole layer and as a likely substrate for the pink lake (see Fig. 4e). If we focus the attention on the green acanthus leaf in the lower right corner, then the lead white highlights are clearly visible in Figs. 11e-f, whereas the presence of azurite throughout the leaf is evident from Figs. 11c-d. The Pb map of Fig. 11e also demonstrates that a significant amount of lead is (fairly uniformly) present, alongside copper, in the green areas of this leaf. The Pb content of this leaf is visible in the Pb-M MA-XRF maps as well (see Fig. 11g), suggesting that the Pb is present at or close by the paint surface, in a mixture with other materials. Faint bands can be isolated in the FTIR data near 450-485 cm^{-1} (and also at 395-445 cm^{-1}); their intensity distribution (Fig. 11h) matches the shape of the green portion of this acanthus leaf. This suggests that the green paint was obtained by mixing blue azurite with a yellow pigment, in this case massicot (PbO), a standard practice employed in 15th c. Florentine workshops.

3.7. Binding media

FORS analysis found spectral evidence for the use of a lipidic binder in areas painted with red lead. The spectral signature is characterized by two relatively weak bands at 2311 and 2352 nm [30], possibly suggesting that whole egg was used rather than egg

yolk, or else that a small amount of egg yolk was added to another type of binder, perhaps to improve the handling properties of the paint.

(MA-)rFTIR was employed to support and possibly refine this identification. All point-based FTIR spectra show intense bands in the 1900-1400 cm^{-1} range, where the absorptions of the main groups in lipids, proteins and polysaccharides can be identified [42]. These spectra differ due to the physical properties of the pictorial layer; sometimes two sharp, almost derivative like signals are present, sometimes they show only a broad peak, with two or more relative maxima. In both cases, these signals can be attributed to the presence of a protein-containing binder. The absence of distinctive peaks at 4329 and 4259 cm^{-1}, attributable to the combination of CH_2 stretching and bending vibrational modes [43] in lipid fatty chains, exclude the use of a pure lipidic binder such as egg yolk.

In the spectra where the derivative-like distortion is predominant (Figure 12b), the two peaks with inflection point at 1652 and 1549 cm^{-1} can be attributed to the amide I and II stretching in proteinaceous binders. These bands are well detectable as relative maxima in the spectra where the derivative distortion is less evident (Figure 12c). When comparing Fig. 12a with 12c, no striking differences can be seen between a spectrum that is recreated from the MA-rFTIR datacube (Fig. 12a) and one obtained by measuring over a longer period in only one position (Fig. 12c).

Further analysis does not reveal the presence of strong C=O stretching absorption, centered around 1740 cm^{-1}, superimposed to the Amide I band. A weak band at 1738 cm^{-1} can be assigned to the $\nu_1 + \nu_4$ carbonate combination band of lead white [28].

When these amide bands are employed to map the distribution of the binding medium in Fig. 12d, surprisingly not all painted areas appear. Mainly the carbonate rich zones (calcite, lead white and azurite) show low amide intensities. When combining the two most abundant carbonate species in Figure 12e: lead white and calcite, the painted areas appear as the inverse of the combined amide band distribution. This is not a surprise since carbonates have active bands in the same spectral region as the amides. Contrary to ATR and transmission spectra, external reflectance bands are often broader because the instrument captures not only specularly reflected radiation, but diffuse reflected radiation as well. The presence of the carbonates changes the physical

properties of the pictorial layers and increases the diffuse reflection component. This diffuse reflection enhances the CO_3^{2-} overtone and combination bands which overlap with the amide bands, making it more difficult to map the amide bands.

This case illustrates that the method to map chemical bands, obtained by MA-rFTIR still has room for improvement. Especially in areas where overlapping bands occur while in the same locations also the spectral background changes, the separation of the net signals of all molecular contributions is difficult to perform in a reliable manner.

4. Conclusions

By employing MA-XRF and MA-rFTIR scanning as complementary, non-invasive spectroscopic means of investigation, we obtained several new types of information about a 15th century Florentine illuminated fragment used as a case study. In general, while MA-XRF allows to image the distribution of the different painters' materials with sufficient lateral detail, it lacks in specificity to unambiguously identify all materials present. For this purpose, a combined investigation with more specific spectroscopic methods based on vibrational interactions such as FTIR or Raman spectroscopy is recommended.

Specifically for this case, the combination of MA-XRF and MA-rFTIR imaging allowed to obtain information on the different types of gilding employed, which included mainly gold leaf applied on a bole substrate, complemented by painting of smaller areas with mosaic gold. Several different lead compounds were identified, such as lead white and minium in addition to lead tin yellow and massicot. The latter was employed in a mixture with azurite to obtain a green hue, consistent with the Florentine tradition of that period. Two types of blue were identified: azurite as a base layer for the blue areas of the initial and natural (Afghan) ultramarine for St Clement's robe and for dark blue shades and outlines in the initial.

The elemental map for Zn allowed the identification of the Latin text present on the reverse side of the fragment, currently obscured by a cardboard support. This, in turn, revealed significant contextual information about this object, which has been physically separated from its parent book for the last two hundred years.

As our ability to record this type of chemical information about entire illuminations, or series of illuminations, increases, exciting new possibilities open up to study the way in which the use of artists' materials and painting techniques evolved over time and geographically. This without having to rely on physical samples removed from these precious objects. As recent research projects, academic conferences and specialist publications prove, the future of manuscript studies (and of heritage science as a whole) lies in the application of cutting-edge non-invasive imaging methods, and on close

collaboration between all parties concerned: from chemists to art historians, from conservators to imaging scientists [44].

Acknowledgements

The authors wish to thank Dr Stella Panayotova, Keeper of Manuscripts and Printed Books at the Fitzwilliam Museum, for allowing technical analysis of the manuscript fragment, and Dr Suzanne Reynolds, Assistant Keeper of Manuscripts and Printed Books, for crucial help in identifying the text of the reverse of the fragment and its significance. We also wish to thank Prof. Andrew Beeby and Dr Catherine Nicholson for their complementary Raman analyses. The warm hospitality of the Hamilton Kerr Institute is also gratefully acknowledged. The Esmée Fairbairn Collections Fund and Cambridge University's Returning Carers Scheme provided funding for part of this research. SL and KJ acknowledge support from project METOX (contract BR/165/A6/MetOx), BELSPO, Brussels.

Figure and table legends

Figure 1: Don Silvestro dei Gherarducci, *St Clement in a historiated initial D*, Florence, c. 1370-1375, 170 x 165 mm. Fitzwilliam Museum, MS 5-1979 (c) The Fitzwilliam Museum, Cambridge, UK.

Table I: Palette identified on MS 5-1979 prior to MA-XRF and MA-rFTIR scanning.

Figure 2: (a) MA-XRF scanning of MS 5-1979; (b) MA-FTIR scanning of MS 5-1979. In both cases, the measuring head is positioned on a motorized two-dimensional stage while the manuscript fragment is securely mounted on an easel and remains stationary.

Figure 3: Elemental maps obtained by MA-XRF scanning of MS 5-1979. Each image consists of 202,500 pixels (total scan time: 21 hours and 26 minutes).

Figure 4: (a) Schematic cross-sectional buildup of gilded areas; b) RGB composite image where R: Fe-K, G: Au-L and B: Ca-K MA-XRF distributions; (c-d) Fe-K and Ca-K distributions, with grey scale adjusted relative to Figure 3 to increase visibility of the lower-intensity areas; (e) FTIR intensity distribution of the 1090-1174 cm^{-1} band, attributed to the sulphate stretching of gypsum ($CaSO_4.2H_2O$).

Figure 5 (a) detail of gilded background in the upper left corner; (b) corresponding false-color map showing locations; in green: covered with a single gold leaf; in yellow: covered with a double thickness of gold leaf; in red: no longer covered by gold leaf, showing an increased Ca-K signal and in blue: other Ca-rich areas (see also Figure 6); (c) detail of the gilded edge of the Saint's robe; (d) corresponding Au-L elemental distribution; (e) detail of orange decoration with lead white highlights showing a dark degradation product.

Figure 6: (a) False color map and (b) Au-L vs. Ca-K correlation plot highlighting the different types and conditions of gilded areas: green pixels: covered with a single gold leaf; yellow: covered with a double thickness of gold leaf; red pixels: losses in the gold leaf, showing low Au and high Ca signals; blue pixels: other high-Ca signal locations.

Figure 7: (a) RGB composite of MA-XRF maps with R: Hg-L, G: Zn-K and B: Fe-K; (b) horizontally mirrored Zn-K map with adjusted contrast settings, improving the readability of the writing on the verso.

Figure 8: (a) Correlation biplot of Pb-L and Sn-L MA-XRF intensity values in MS 5-1979; (b) Pb-L elemental distribution; (c) false color Pb-L image, based on the groups indicated in the correlation biplot; (d-e) FTIR intensity maps attributed to (d) carbonate bending mode of Lead White (680-720 cm^{-1}) and (e) Pb-O stretch of Minium (530-585 cm^{-1}).

Figure 9: (a) Detail of left side of the initial D showing different blue tones; (b) virtual cross-section over the red line indicated in (a), representing the layer buildup in this area; (c-d-e) corresponding Cu-K, Ca-K and K-K MA-XRF maps; (f) microphotograph of area indicated by yellow rectangle in (a).

Figure 10: Fitzwilliam Museum, MS 5-1979: (a) MA-XRF K-K distribution; (b-c-d) FTIR intensity distributions: (b) CO_2 or HS_3^- stretching (2317-2362 cm^{-1}), signaling the presence of Afghan ultramarine; (c) Si-O bending (465-530 cm^{-1}) and (d) Si-O stretching (960-1050 cm^{-1}), both attributed to ultramarine blue and/or other silicates.

Figure 11: Fitzwilliam Museum, MS 5-1979; Top row: MA-XRF elemental distributions: (a) Ca-K; (c) Cu-K; (e) Pb-L; (g) Pb-M; Bottom row: FTIR intensity distributions: (b) carbonate combination band of chalk (1777-1818 cm^{-1}); (d) carbonate combination band of azurite (4220-4290 cm^{-1}); (f) carbonate bending mode of lead white (680-720 cm^{-1}); (h) combination of two Pb-O stretching bands of massicot (395-445 and 450-485 cm^{-1}).

Figure 12: Reflection mode spectra in the region 4500-375 cm^{-1} of (a) the blue initial (spectrum extracted from the MA-rFTIR datacube), the arrow points out the distinctive peak for genuine Afghan ultramarine; (b) the green earth over the white alb; (c) the blue region in the initial; MA-rFTIR intensity distributions of (d) combined intensities of Amide I and Amide II bands; (e) combined intensities of the carbonate bending mode of lead white (680-720 cm^{-1}) and the carbonate combination band of chalk (1777-1818 cm^{-1}).

References

[1] M. Aceto, A. Agostino, G. Fenoglio, A. Idone, M. Gulmini, M. Picollo, P. Ricciardi, J.K. Delaney, Characterisation of colourants on illuminated manuscripts by portable fibre optic UV-visible-NIR reflectance spectrophotometry, Anal. Methods. 6 (2014) 1488-1500 https://doi.org/10.1039/c3ay41904e

[2] C. Anselmi, P. Ricciardi, D. Buti, A. Romani, P. Moretti, K.R. Beers, B.G. Brunetti, C. Miliani, A. Sgamellotti, MOLAB® meets Persia: Non-invasive study of a sixteenth-century illuminated manuscript Stud. Conserv. 60 (2015) 185-191 https://doi.org/10.1179/0039363015Z.000000000223

[3] B. Doherty, A. Daveri, C. Clementi, A. Romani, S. Bioletti, B. Brunetti, A. Sgamellotti, C. Miliani, The book of Kells: A non-invasive MOLAB investigation by complementary spectroscopic techniques, Spectrochim. Acta A 115 (2013) 330-336 https://doi.org/10.1016/j.saa.2013.06.020

[4] D. Lauwers, V. Cattersel, L. Vandamme, A. Van Eester, K. De Langhe, L. Moens and P. Vandenabeele, Pigment identification of an illuminated mediaeval manuscript De Civitate Dei by means of a portable Raman Equipment, J. Raman Spectrosc. 45 (2014) 1266-1271 https://doi.org/10.1002/jrs.4500

[5] W. Faubel, S. Staub, R. Simon, S. Heissler, A. Pataki, G. Banik, Non-destructive analysis for the investigation of decomposition phenomena of historical manuscripts and prints, Spectrochim. Acta B 62 (2007) 669-676 https://doi.org/10.1016/j.sab.2007.03.029

[6] M.J. Melo, A. Claro, Bright light: microspectrofluorimetry for the characterization of lake pigments and dyes in works of art, Acc. Chem Res. 43 (2010) 857-866 https://doi.org/10.1021/ar9001894

[7] G. Van der Snickt, W. De Nolf, B. Vekemans, K. Janssens, µ-XRF/µ-RS vs. SR µ-XRD for pigment identification in illuminated manuscripts, Appl. Phys. A 92 (2008) 59-68 https://doi.org/10.1007/s00339-008-4447-9

[8] A. Duran, J.L. Perez-Rodriguez, T. Espejo, M.L. Franquelo, J. Castaing, P. Walter, Characterization of illuminated manuscripts by laboratory-made portable XRD and micro-XRD systems, Anal. Bioanal. Chem. 395 (2009) 1997-2004 https://doi.org/10.1007/s00216-009-2992-5

[9] A. Duran, A. López-Montes, J. Castaing, T. Espejo, Analysis of a royal 15th century illuminated parchment using a portable XRF-XRD system and micro-invasive techniques, J. Archaeol. Sci. 45 (2014) 52-58 https://doi.org/10.1016/j.jas.2014.02.011

[10] M. Borengasser, W.S. Hungate, R. Watkins, Hyperspectral remote sensing - Principles and applications, CRC press, 2007

[11] C. Balas, V. Papadakis, N. Papadakis, A. Papadakis, E. Vazgiouraki, G. Themelis, A novel hyper-spectral imaging apparatus for the non-destructive analysis of objects of artistic and historic value, J. Cult. Herit. 4 (2003) 330-337 https://doi.org/10.1016/S1296-2074(02)01216-5

[12] K.C. Gross, K.C. Bradley, G.P. Perram, Remote identification and quantification of industrial smokestack effluents via imaging Fourier-transform spectroscopy, Environ. Sci. Technol. 44 (2010) 9390-9397 https://doi.org/10.1021/es101823z
[13] F. Rosi, C. Miliani, R. Braun, R. Harig, D. Sali, B. G. Brunetti, A. Sgamellotti, Noninvasive analysis of paintings by Mid-infrared hyperspectral imaging, Angew. Chem. Int. Ed. 52 (2013) 1-5 https://doi.org/10.1002/anie.201209929
[14] K.A. Dooley, D.M. Conover, L.D. Glinsman, J.K. Delaney, Complementary standoff chemical imaging to map and identify artist materials in an early Italian Renaissance panel painting, Angew. Chem. 126 (2014) 13995-13999 https://doi.org/10.1002/ange.201407893
[15] K.A. Dooley, J. Coddington, J. Krueger, D.M. Conover, M. Loew, J.K. Delaney, Standoff chemical imaging finds evidence for Jackson Pollock's selective use of alkyd and oil binding media in a famous 'drip' painting, Anal. Methods 9 (2017) 28-37 https://doi.org/10.1039/c6ay01795a
[16] M. Alfeld, K. Janssens, J. Dik, W. De Nolf, G. Van der Snickt, Optimization of mobile scanning macro-XRF systems for the in situ investigation of historical paintings, J. Anal. At. Spectrom. 26 (2011) 899–909 https://doi.org/10.1039/c0ja00257g
[17] S. Legrand, F. Vanmeert, G. Van der Snickt, M. Alfeld, W. De Nolf, J. Dik, K. Janssens, Examination of historical paintings by state-of-the-art hyperspectral imaging methods: from scanning infra-red spectroscopy to computed X-ray laminography, Herit. Sci. 2 (2014) 13 https://doi.org/10.1186/2050-7445-2-13
[18] W. Vetter, M. Schreiner, A fiber optic reflection-UV/Vis/NIR-system for non-destructive analysis of art objects¸ Adv. Chem. Sci. 3 (2014) 7-14
[19] M. Alfeld, G. Van der Snickt, F. Vanmeert, K. Janssens, J. Dik, K. Appel, L. van der Loeff, M. Chavannes, T. Meedendorp, E. Hendriks, Scanning XRF investigation of a Flower Still Life and its underlying composition from the collection of the Kröller-Müller Museum, App. Phys. A 111 (2013) 165-175 https://doi.org/10.1007/s00339-012-7526-x
[20] G. Van der Snickt, H. Dubois, J. Sanyova, S. Legrand, A. Coudray, C. Glaude, M. Postec, P. Van Espen, K. Janssens, Large-area elemental imaging reveals Van Eyck's original paint layers on the Ghent Altarpiece (1432), rescoping its conservation treatment, Angew. Chem. 56 (2017) 4797-4801 https://doi.org/10.1002/anie.201700707
[21] S. Legrand, M. Alfeld, F. Vanmeert, W. De Nolf, K. Janssens, Macroscopic Fourier transform infrared scanning in reflection mode (MA-rFTIR), a new tool for chemical imaging of cultural heritage artefacts in the mid-infrared range, Analyst 139 (2014) 2489-2495 https://doi.org/10.1039/c3an02094k
[22] S. Panayotova (ed.), Colour. The Art and Science of Illuminated Manuscripts. Harvey Miller/Brepols, London and Turnhout 2016, pp. 139-142 See also http://www.fitzmuseum.cam.ac.uk/illuminated/manuscript/discover/initials-from-choir-books
[23] M. Levi D'Ancona, The illuminators and illuminations of the choir books from Santa Maria degli Angeli and Santa Maria Nuova in Florence, vol. 1, Centro Di, Florence, 1994, pp. 91

[24] M. Alfeld and K. Janssens, Strategies for processing mega-pixel X-ray fluorescence hyperspectral data: a case study on a version of Caravaggio's painting Supper at Emmaus, J. Anal. At. Spectrom. 30 (2015) 777-789 https://doi.org/10.1039/c4ja00387j
[25] V.A. Solé, E. Papillon, M. Cotte, Ph. Walter, J. Susini, A multiplatform code for the analysis of energy-dispersive X-ray fluorescence spectra, Spectrochim. Acta Part B 62 (2006) 63–68 https://doi.org/10.1016/j.sab.2006.12.002
[26] Brightspec NV, http://www.brightspec.be, Belgium
[27] A. Cabal, S. Legrand, B. Van den Bril, K. Toté, K. Janssens, P. Van Espen, Study of the uniformity of aerosol filters by scanning MA-XRF, X-Ray Spectrom. 46 (2017) 461-466 https://doi.org/10.1002/xrs.2767
[28] C. Miliani, F.Rosi, A. Daveri, B.G. Brunetti, Reflection infrared spectroscopy for the non-invasive in situ study of artists' pigments, App. Phys. A 106 (2012) 295-307 https://doi.org/10.1007/s00339-011-6708-2
[29] P. Ricciardi, MS 5-1979 – Summary of analytical results, unpublished technical analysis report, 10 August 2015
[30] P. Ricciardi, J.K. Delaney, M. Facini, J.G. Zeibel, M. Picollo, S. Lomax, M. Loew, Near-Infrared Reflectance imaging spectroscopy to map paint binders in situ on illuminated manuscripts, Angew. Chem. Int. Ed., 51 (2012) 5607-610 https://doi.org/10.1002/anie.201200840
[31] P. Ricciardi, M. Facini, J. Delaney, Painting and illumination in Early Renaissance Florence: the techniques of Lorenzo Monaco and his workshop, in The Renaissance Workshop, Ed. D. Saunders, M. Spring, A. Meek, London, 2013, 1-9
[32] M. Vermeulen, J. Sanyova, K. Janssens, G. Nuyts, S. De Meyer, K. De Wael, The darkening of copper- or lead-based pigments explained by a structural modification of natural orpiment: a spectroscopic and electrochemical study, J. Anal. At. Spectrom. 32 (2017) 1331-1341 https://doi.org/go10.1039/c7ja00047b
[33] D. Goltz, J. McClelland, A. Schellenberg, M. Attas, E. Cloutis, C. Collins, Spectroscopic studies on the darkening of lead white, App. Spectrosc. 57 (2003) 1393-1398
[34] G. Smith, A. Derbyshire, R.J.H. Clark, In situ spectroscopic detection of lead sulphide on a blackened manuscript illumination by Raman microscopy, Stud. Conserv. 47 (2002) 250-256 https://doi.org/10.1179/sic.2002.47.4.250
[35] A. Coccato, L. Moens, P. Vandenabeele, On the stability of mediaeval inorganic pigments: a literature review of the effect of climate, material selection, biological activity, analysis and conservation treatments, Herit. Sci. 5 (2017) https://doi.org/10.1186/s40494-017-0125-6
[36] N Turner, K. Trentelman, C. Patterson, J. Dik, G. Van der Snickt, K. Janssens, Macro-XRF Scanning of Illuminations: An improved method for non-invasive analysis of illuminated manuscripts, Proceedings of "INSIDE ILLUMINATIONS. Art Technical Research & the Illuminated Manuscript", KIK-IRPA, Brussels, 5 June 2014, Corpus of Illuminated Manuscripts of Illuminare, KU Leuven, Peeters Publishers, Leuven (2015) (forthcoming)
[37] S. Legrand, P. Ricciardi and K. Janssens, 'The benefits of scanning illuminated manuscripts with MA-XRF and MA-rFTIR', in S. Panayotova and P. Ricciardi (eds),

Manuscripts in the Making: Art and Science, vol. 2, Harvey Miller/Brepols, forthcoming 2018
[38] W.B. White, The carbonate minerals in the infrared spectra of minerals, V.C. Farmer, Mineralogical Society of Great Britain and Ireland, 1974, pp 227-283. https://doi.org/10.1180/mono-4
[39] S. Vahur, U. Knuutinen, I. Leito, ATR-FT-IR spectroscopy in the region of 500–230 cm^{-1} for identification of inorganic red pigments, Spectrochim. Acta Part A 73 (2009) 764-771 https://doi.org/10.1016/j.saa.2009.03.027
[40] C. Miliani, A. Daveri, B. G. Brunetti, A. Sgamellotti, CO_2 entrapment in natural ultramarine blue, Chem. Phys. Lett. 466 (2008) 148-151 https://doi.org/10.1016/j.cplett.2008.10.038
[41] M. Bacci, C. Cucci, E. Del Federico, A. Lenco, A. Jerschow, J.M. Newman, M. Picollo, An integrated spectroscopic approach for the identification of what distinguishes Afghan lapis lazuli from others, Vib. Spectrosc. 49 2009 80-83 https://doi.org/10.1016/j.vibspec.2008.05.002
[42] R. Arbizzani, U. Casellato, E. Fiorin, L. Nodari, U. Russo, P.A. Vigato, Decay markers for the preventive conservation and maintenance of paintings, J. Cult. Herit. 5 (2004), 167-182 https://doi.org/10.1016/j.culher.2003.12.003
[43] M. Vagnini, C. Miliani, L. Cartechini, P. Rocchi, B.G. Brunetti, A. Sgamellotti, Anal. Bioanal. Chem. 395 (2009) 2107–2118 https://doi.org/10.1007/s00216-009-3145-6
[44] S. Panayotova and P. Ricciardi (eds), Manuscripts in the Making: Art and Science, 2 volumes, Harvey Miller/Brepols, forthcoming 2017-2018


a
b

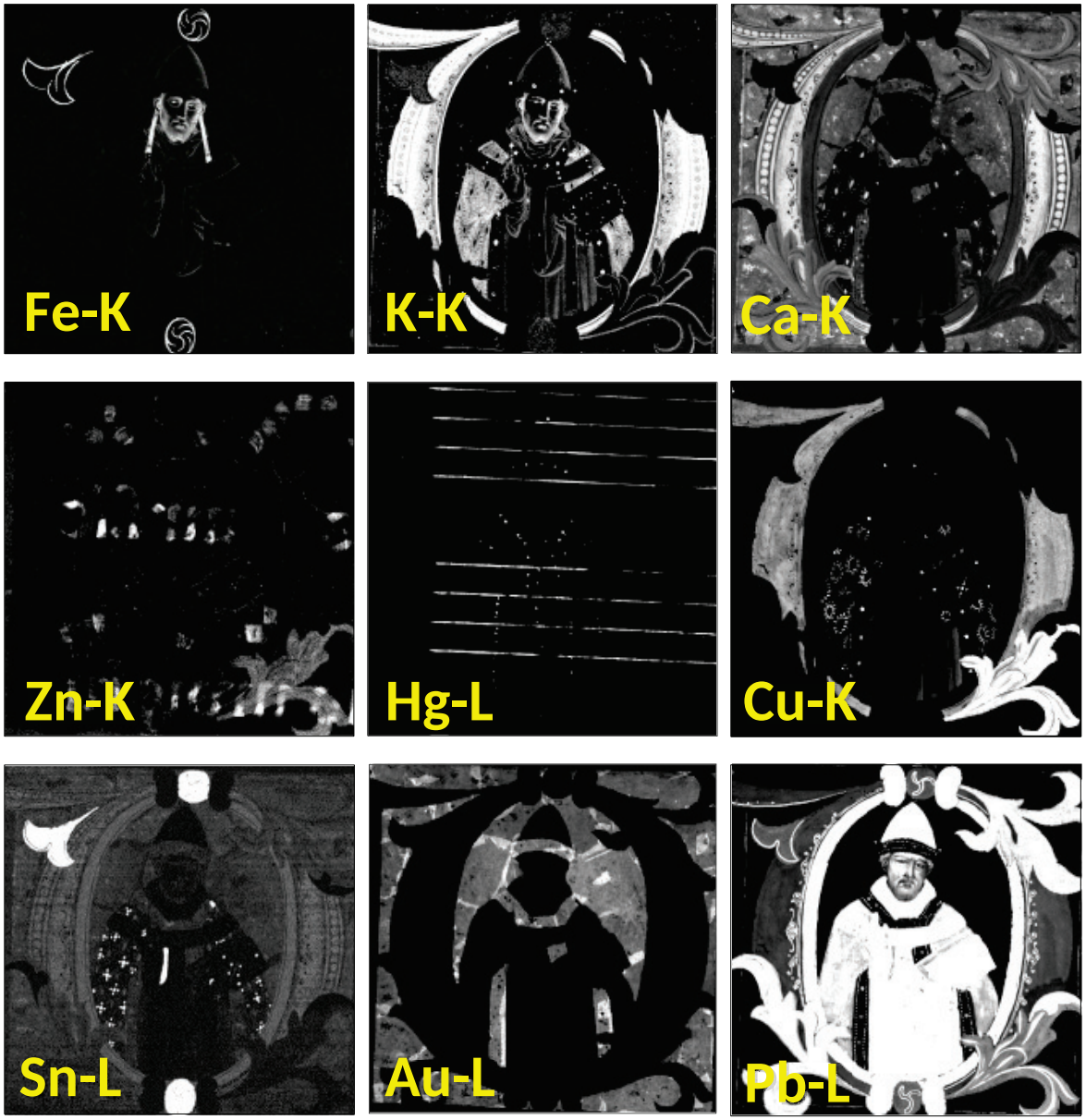
Fe-K
K-K
Ca-K
Zn-K
Hg-L
Cu-K
Sn-L
Au-L
Pb-L

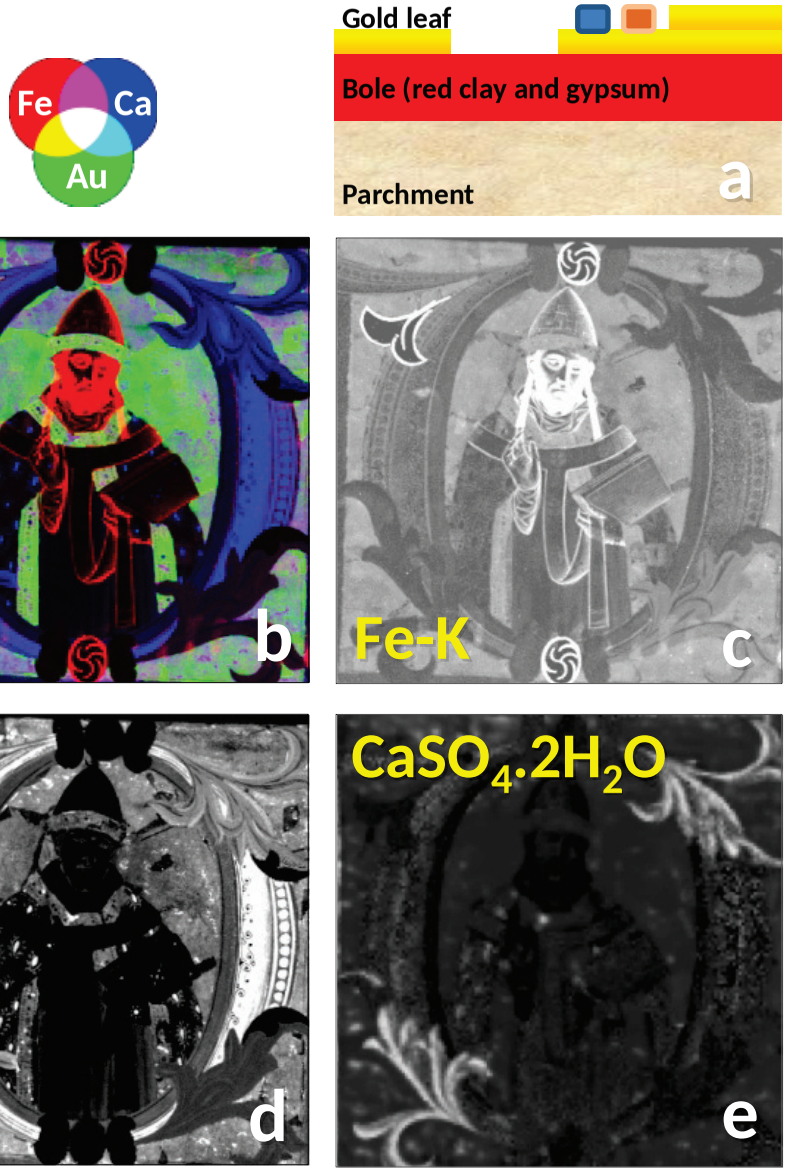
Fe
Ca
Au
Gold leaf
Bole (red clay and gypsum)
Parchment
a
b
Fe-K
c
Ca-K
d
$CaSO_4.2H_2O$
e

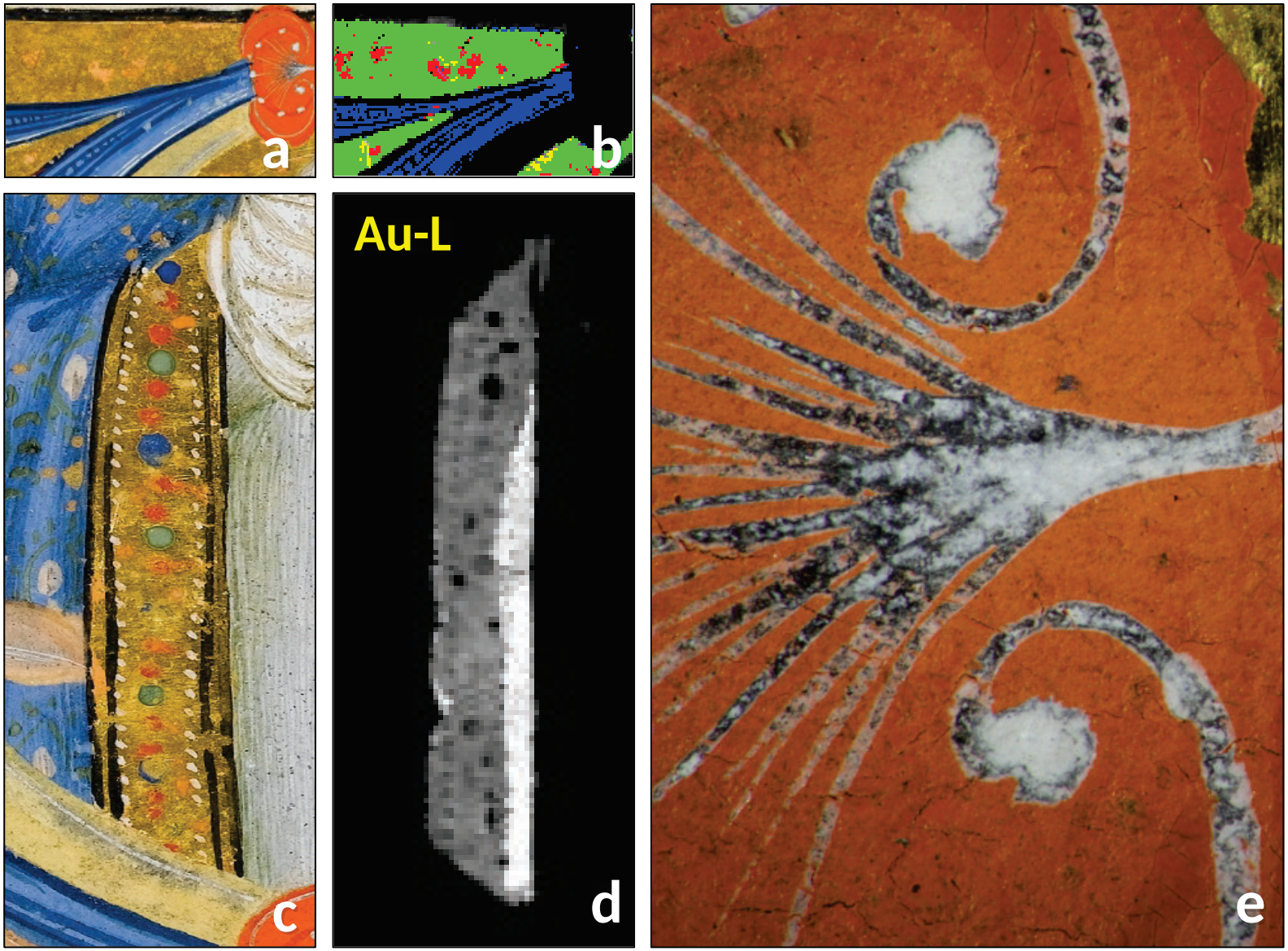
a
b
Au-L
d
e

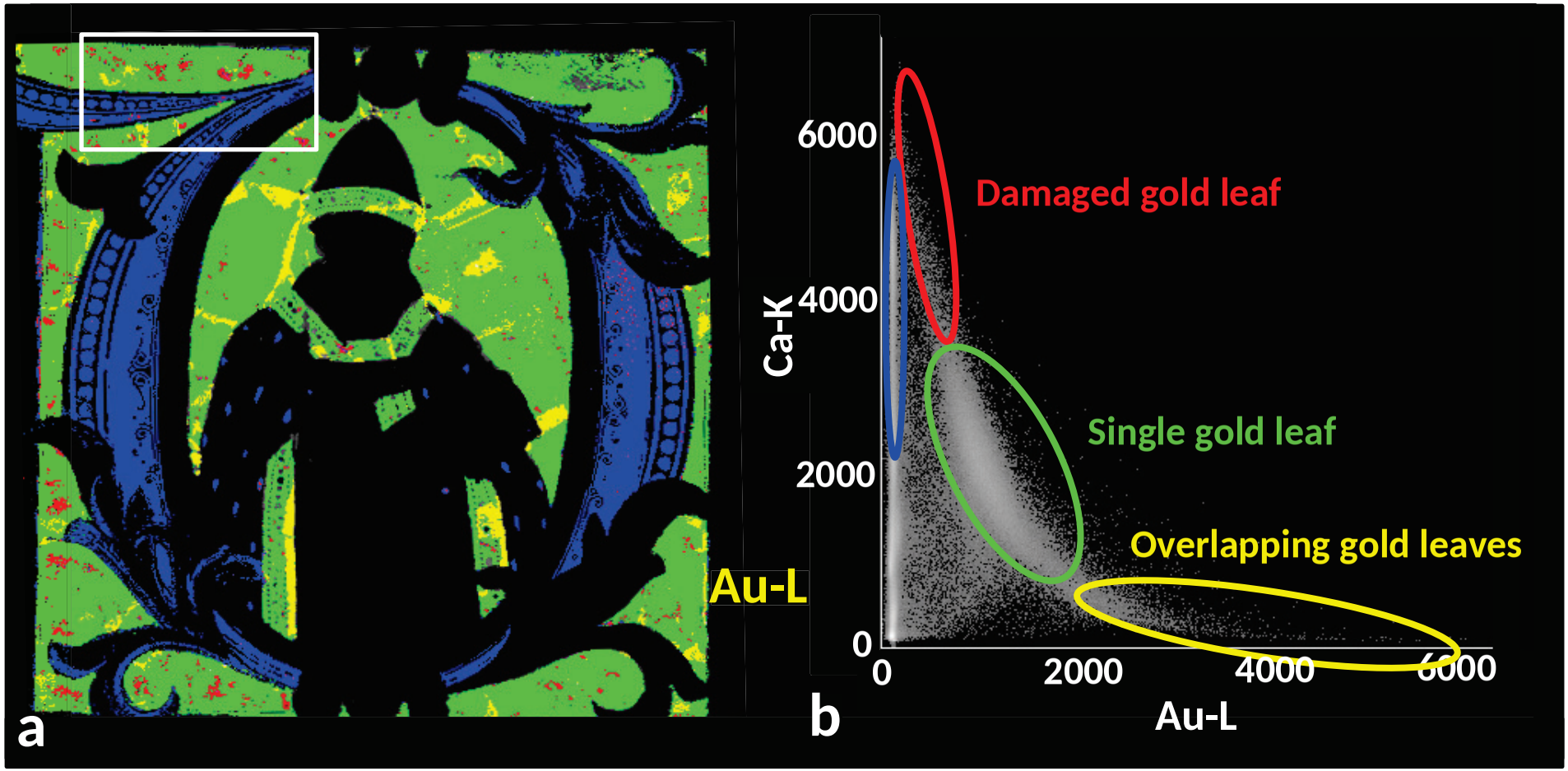
a
Au-L
b
Ca-K
6000
4000
2000
0
0
2000
4000
6000
Au-L
Damaged gold leaf
Single gold leaf
Overlapping gold leaves

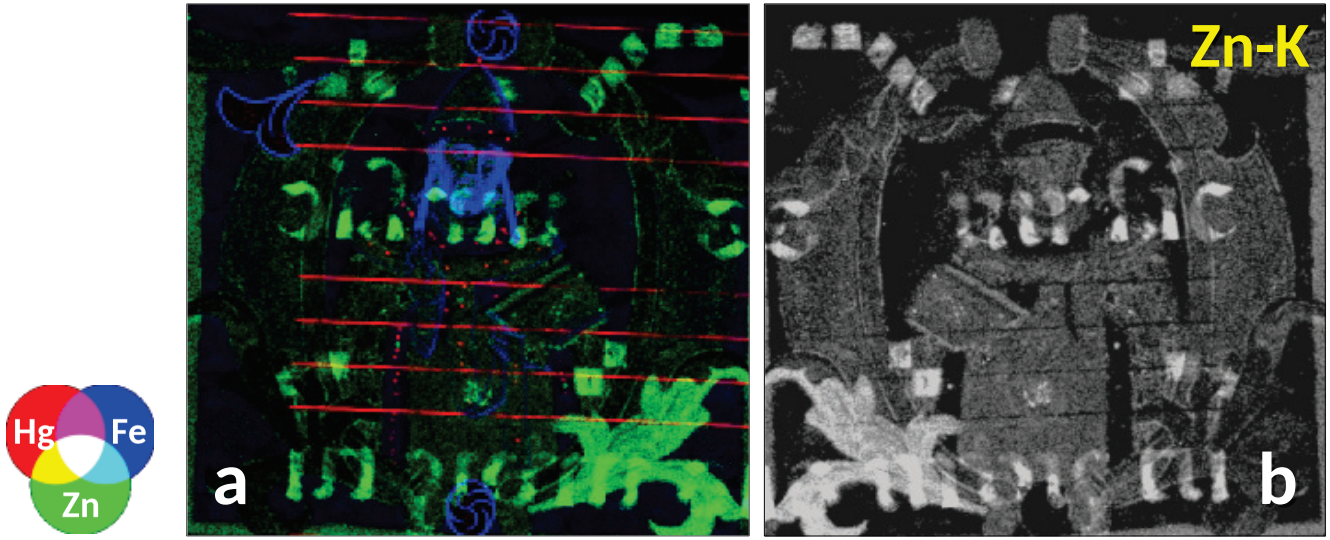
Hg
Fe
Zn
a
Zn-K
b

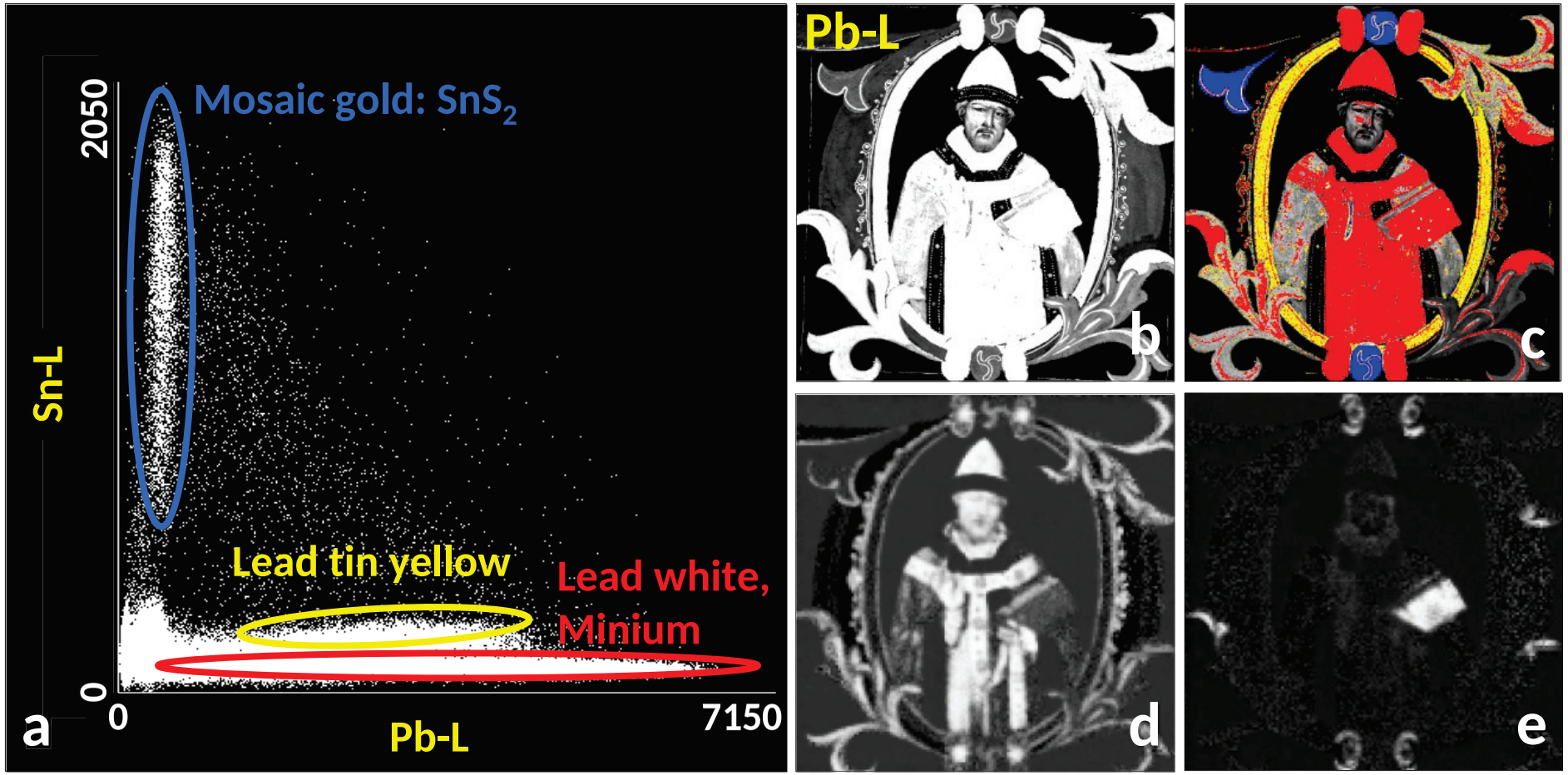
Mosaic gold: SnS_2
Lead tin yellow
Lead white,
Minium
Sn-L
2050
0
0
7150
Pb-L
a
Pb-L
b
c
d
e

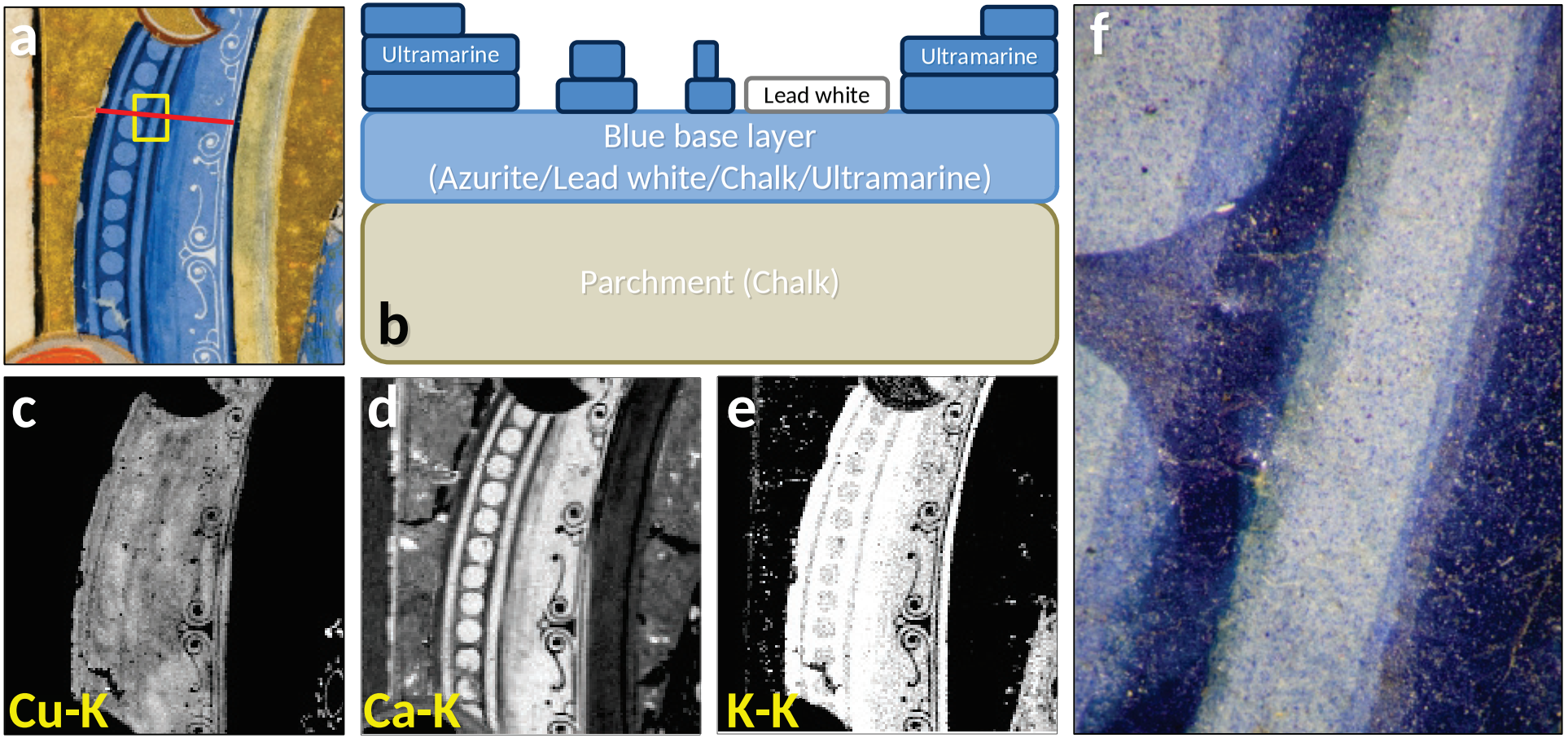
a
Ultramarine
Lead white
Ultramarine
Blue base layer
(Azurite/Lead white/Chalk/Ultramarine)
Parchment (Chalk)
b
f
c
Cu-K
d
Ca-K
e
K-K

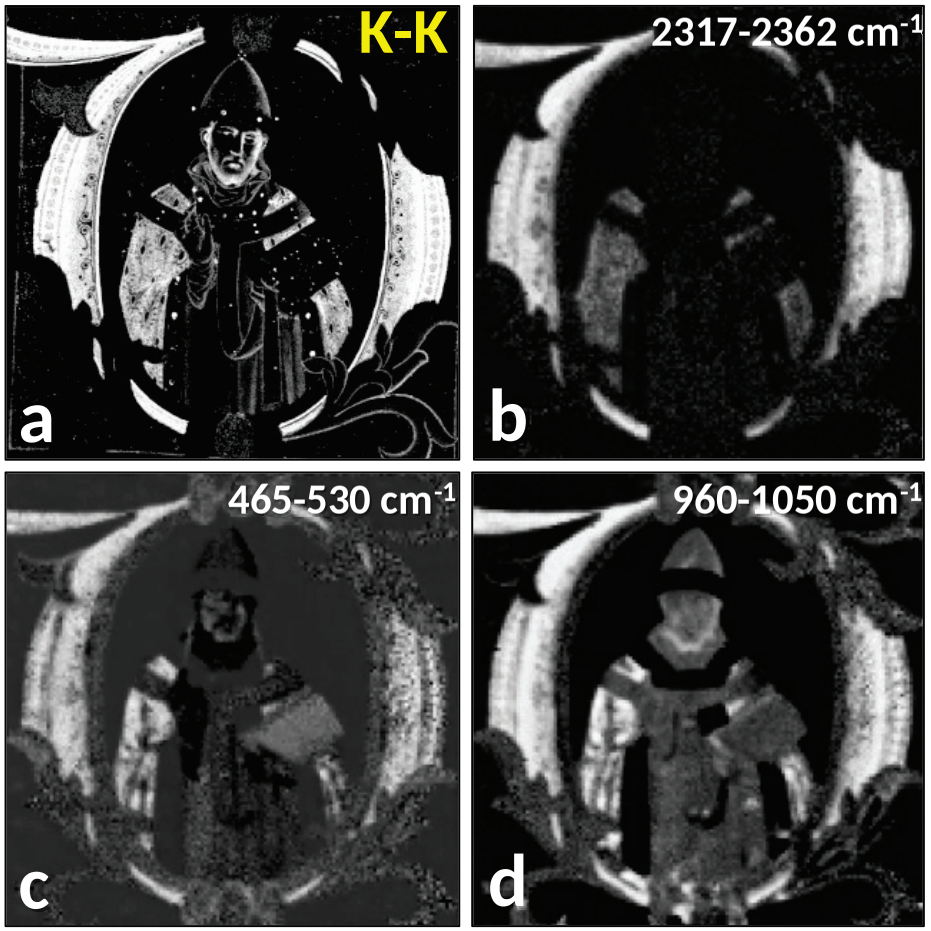
K-K
a
2317-2362 cm-1
b
465-530 cm-1
c
960-1050 cm-1
d

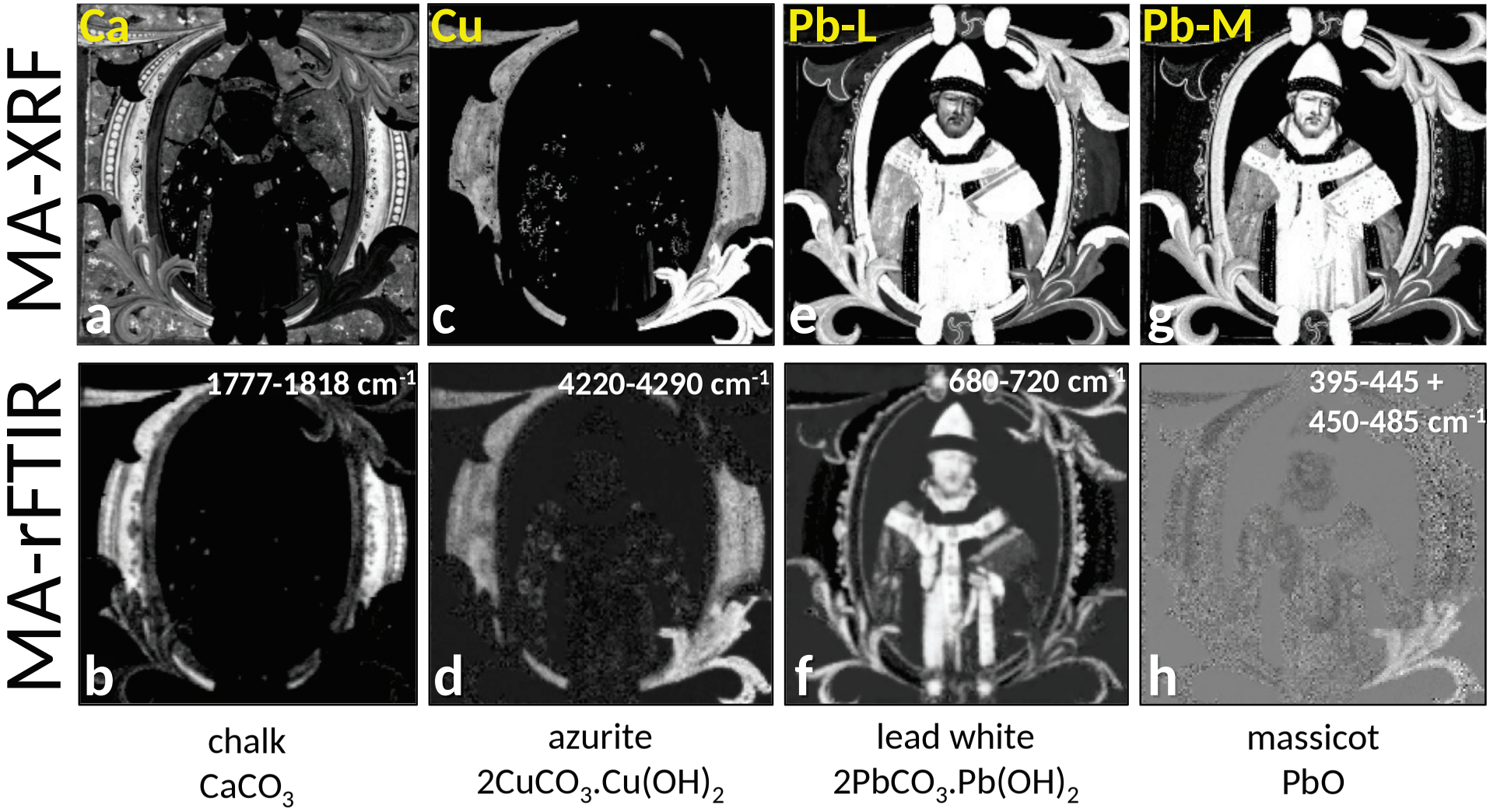
MA-XRF
MA-rFTIR
Ca
Cu
Pb-L
Pb-M
a
c
e
g
1777-1818 cm-1
4220-4290 cm-1
680-720 cm-1
395-445 +
450-485 cm-1
b
d
f
h
chalk
CaCO3
azurite
2CuCO3.Cu(OH)2
lead white
2PbCO3.Pb(OH)2
massicot
PbO

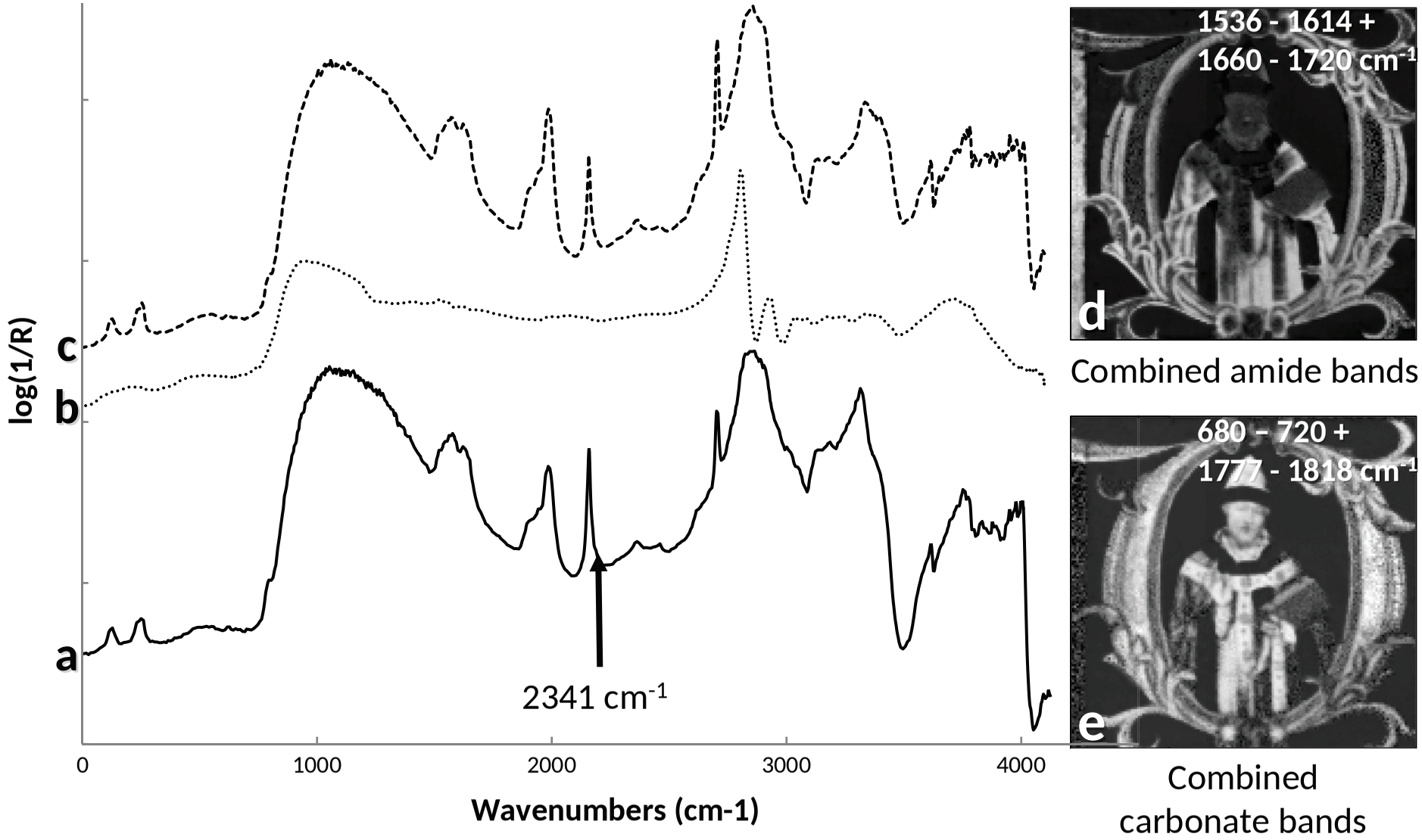
log(1/R)
c
b
a
2341 cm-1
0
1000
2000
3000
4000
Wavenumbers (cm-1)
1536 - 1614 +
1660 - 1720 cm-1
d
Combined amide bands
680 – 720 +
1777 - 1818 cm-1
e
Combined
carbonate bands